SPECTRAL CONSTRAINTS FOR MILLISECOND PULSARS DUE TO GENERAL RELATIVISTIC FRAME DRAGGING

C. VENTER and O.C. DE JAGER

Unit for Space Physics, North-West University, Potchefstroom Campus, Potchefstroom, South Africa; E-mail: fskcv@puk.ac.za

Abstract. We develop a numerical code for simulating the magnetospheres of millisecond pulsars, which are expected to have unscreened electric potentials due to the lack of magnetic pair production. We incorporate General Relativistic (GR) expressions for the electric field and charge density and include curvature radiation (CR) due to primary electrons accelerated above the stellar surface, whereas inverse Compton scattering (ICS) of thermal X-ray photons by these electrons are neglected as a second-order effect. We apply the model to PSR J0437-4715, a prime candidate for testing the GR-Electrodynamic theory, and find that the curvature radiation spectrum cuts off at energies below 15 GeV, which are well below the threshold of the H.E.S.S. telescope, whereas Classical Electrodynamics predict a much higher cutoff near 100 GeV, which should be visible for H.E.S.S., if standard assumed Classical Electrodynamics apply. GR theory also predicts a relatively narrow pulse ($2\phi_L \sim 0.2$ phase width) centered on the magnetic axis, which sets the beaming solid angle to $\sim$0.5 sr per polar cap (PC) for a magnetic inclination angle of 35° relative to the spin axis, given an observer which sweeps close to the magnetic axis. We also find that EGRET observations above 100 MeV of this pulsar constrain the polar magnetic field strength to $B_{\rm pc} < 4 \times 10^8$ G for a pulsar radius of 10 km and moment of inertia of 10^{45} g cm^2. The field strength constraint becomes even tighter for a larger radius and moment of inertia. Furthermore, a reanalysis of the full EGRET data set of this pulsar, assuming the predicted pulse shape and position, should lead to even tighter constraints on neutron star and GR parameters, up to the point where the GR-derived potential and polar cap current may be questioned.

Keywords: stars: neutron, pulsars: individual (PSR J0437-4715)

1. Introduction

It has been noted by several authors (e.g. Muslimov and Harding, 1997; Dyks et al., 2001) that General Relativistic (GR) frame dragging in rotating neutron stars is a first-order effect, which has to be included in a self-consistent model of pulsar magnetospheric structure and associated radiation, and transport processes. Many efforts were directed towards this end.

Usov (1983) was the first to suggest that the low magnetic field strengths of millisecond pulsars allow gamma-rays up to at least 100 GeV to escape magnetic pair production. Subsequent evaluation (Harding et al., 2002 [HMZ02]) have shown that most millisecond pulsars have unscreened electric fields due to the low optical depths of primary curvature gamma-rays for magnetic pair production in such

low-B pulsar magnetospheres. Radiation reaction limited curvature gamma-rays up to about 100 GeV from millisecond pulsars were predicted (Bulik et al., 2000; HMZ02), making nearby millisecond pulsars such as PSR J0437-4715 (Johnston et al., 1993) attractive targets for ground-based gamma-ray groups (Bulik et al., 2000; Venter, 2004). The unscreened case offers a test for fundamental GR electrodynamical derivations of the polar cap current and potential, without having to invoke additional modifications such as pair formation fronts (Harding and Muslimov, 1998) with associated slot gaps (Muslimov and Harding, 2003) to explain most observations of canonical (high-B) pulsars.

The assumption that no screening takes place was indeed validated *a posteriori* and is also supported by the fact that PSR J0437-4715 has a relatively low spindown power, inhibiting magnetic pair production (HMZ02). This means that the value of the GR-derived parallel electric field may be used with confidence (see Section 2.1). Secondly, several important parameters, most notably the mass and distance (Van Straten et al., 2001), are known to a high degree of accuracy (see Figure 1 for a list of parameters used). Thirdly, PSR J0437-4715 is one of the closest pulsars to Earth, lying at a distance of 139 ± 3 pc (Van Straten et al., 2001). PSR J0437-4715 may therefore be expected to be much brighter and more easily observable than other millisecond pulsars. Lastly, observations show that the radio and X-ray beams virtually coincide, implying that the observer's line of site cuts the PC near the magnetic axis, providing certainty about geometric constraints. In fact, Manchester and Johnston

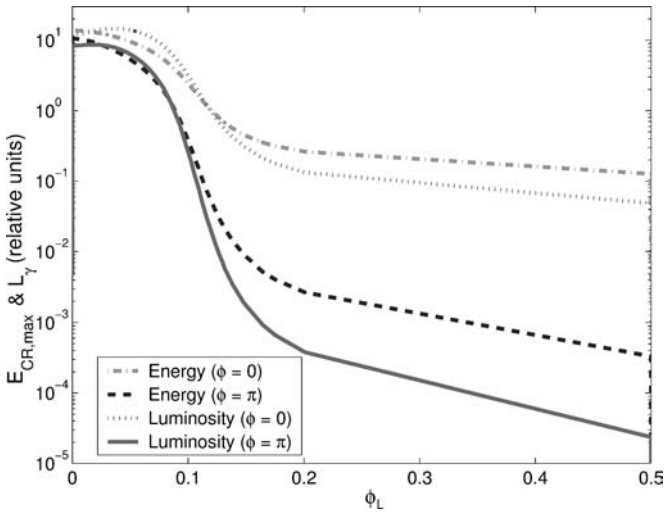

Figure 1. Maximum CR photon energy and photon luminosity (in relative units) vs. observer pulse phase for half a rotation period (with phase zero corresponding to the radio pulse maximum) for PSR J0437-4715, for magnetic azimuthal angle $\phi = 0$ and $\phi = \pi$ as indicated in the legend. The following parameters were assumed (Bulik et al., 2000; Van Straten et al., 2001; Zavlin et al., 2002): $P = 5.76 \times 10^{-3}$ s (period), $B_{pc} = 7.4 \times 10^8$ G, $R = 1.6 \times 10^6$ cm (stellar radius), $I = 3 \times 10^{45}$ g cm^2 (moment of inertia), $M = 1.58\ M_{sun}$ and $\chi = 35^\circ$.

(1995) infer a minimum observer angle of 5° with respect to the magnetic axis. The observer, therefore, sweeps through the approximate center of the polar cap.

The effect of GR constraints on millisecond pulsar (MSP) spectral cutoffs is investigated in this paper by simulating (using a finite element approach) radiative and transport processes that occur in a pulsar magnetosphere. One of the most interesting predictions from Muslimov and Harding (1997) is that the primary electron luminosity was predicted to be equal to a quadratic function of the compactness parameter $\kappa = \epsilon I/MR^2$ (with $\epsilon = 2GM/Rc^2$) of the neutron star, times the spin-down power ($\dot{E}_{\rm rot} = I\Omega\dot{\Omega}$, with Ω the angular speed and $\dot{\Omega}$ its time derivative) of the pulsar, giving (assuming that the magnetic and spin axes are aligned):

$$L_{\rm prim,max}^{|\chi=0} \sim \frac{3}{4}\kappa(1-\kappa)\dot{E}_{\rm rot}. \tag{1}$$

2. The Model

Standard classical expressions were employed for the dipole magnetic field and radius of curvature $\rho_{\rm c}$ of an oblique pulsar with magnetic moment μ inclined at an angle $\chi = 35^\circ$ relative to the spin axis (Manchester and Johnston, 1995). GR corrections to these quantities were assumed to be of second order and were therefore not employed. The effect of relativistic frame dragging on the charge density, potential and hence the magnitude of $E_{||}$ (the electric field component parallel to the magnetic field) are however of first order and had to be carefully modelled as prescribed by Harding and Muslimov (1998) for the unscreened case.

2.1. The unscreened electric field

Since the optical depths for magnetic pair production for different regions above the PC are insignificantly small, we use the electric field expressions for the case when there is no screening, i.e. when no upper pair formation front (PFF) forms (Muslimov and Tsygan, 1992; Muslimov and Harding, 1997; Harding and Muslimov, 1998). For the 'near case', we use Eq. (51) of Muslimov and Tsygan (1992), which is equivalent to Eq. (64) of Muslimov and Harding (1997). For the 'far case', we use Eq. (14) of Harding and Muslimov (1998). For purposes of comparison, the 'classic' function of Bulik et al. (2000) as defined in their Eq. (2) was also investigated.

2.2. Radiative and transport processes

The change in the energy of a primary electron is given (when only the dominating CR component is considered, neglecting ICS and synchrotron radiation) by

$$\frac{dE}{dt} = e\beta_r c E_{||} - \frac{2}{3}\left(\frac{e^2 c}{\rho_{\rm c}^2}\right)\gamma^4, \tag{2}$$

with e the electron charge, ρ_c the curvature radius, $\beta_r = v_e/c$ the normalised electron speed (as a function of the radial coordinate r), $E_{||}$ the electric field component parallel to the magnetic field lines and γ the Lorentz factor. The photon energy is set equal to the characteristic CR energy in units of $m_e c^2$ (Luo et al., 2000):

$$\epsilon_\gamma \approx \epsilon_c = \frac{3}{2}\left(\frac{\lambda_c}{\rho_c}\right)\gamma^3, \tag{3}$$

with $\lambda_c = \hbar/m_e c \approx 3.86 \times 10^{-11}$ cm the Compton wavelength. The maximum CR cutoff energy is obtained by inserting a neutron star radius of $R_6 = R/10^6$ cm $= 1.6$ and moment of inertia of $I_{45} = I/10^{45}$ g cm^2 ~ 3 (e.g., HMZ02) for a mass of $M = 1.58\ M_{\rm sun}$ derived from the Shapiro delays (Van Straten et al., 2001). This corresponds to a compactness parameter of $\kappa = 0.11$. We also assume a polar cap field strength corrected for kinematic effects (as assumed by Bulik et al. (2000)) of $B_8 = B_{\rm pc}/10^8$ G $= 7.4$. The relative altitude (radial distance) for maximum CR energy is obtained as $\eta = r/R \sim 1.46$ corresponding to a normalized field line colatitude of $\xi = \theta/\Theta_0 = 0.1$ (with Θ_0 the polar angle of the last closed magnetic field line at the stellar surface) and field line radius of curvature of $\rho_c \sim 6.6 \times 10^7$ cm, while the magnetic azimuth $\phi = 0$ results in a maximum GR potential. Note again that $\chi = 35^\circ$ as derived from radio observations. The analytical expression for the maximum gamma-ray energy is obtained by combining the equation of the 'far' electric field with Eqs. (2) and (3), giving

$$\epsilon_{\gamma,\rm max} = \left(\frac{3}{2}\right)^{7/4} \lambda_c \left(\frac{\beta_r E_{||}}{e}\right)^{3/4}_{\rm max} \rho_c^{1/2} < 15\ \text{GeV}. \tag{4}$$

3. Results

3.1. Energy spectra and fluxes

Since the electrons become relativistic for r slightly larger than R (stellar radius), the bolometric luminosity of a single polar cap will be given by (Muslimov and Harding, 1997)

$$L_{\rm prim} = \alpha c \int |\rho_e| \Phi\, dS, \tag{5}$$

with Φ the electric potential and dS the element of spherical surface cut by the last open field lines at radial distance r. Integrating over ξ and ϕ, and letting $\eta \to \infty$,

we obtain (Venter, 2004)

$$L_{\rm prim,max} = L^{|\chi=0}_{\rm prim,max}\left\{\cos^2\chi + \left(\frac{3\Theta_0 H(1)[\pi/2 - \Theta_0 H(1)]}{16\kappa(1-\kappa)}\right)\sin^2\chi\right\}, \qquad (6)$$

providing we adopt a value of $\Theta(\eta) = \pi/2$ for distances $\eta > c/\Omega R$ (see Eq. (6) of Harding and Muslimov (1998)). This result reduces back to Eq. (1) when χ is set equal to zero.

A value of $\chi = 35^\circ$ implies that the maximum efficiency of conversion of pulsar spindown power into particle luminosity is about 7% for PSR J0437-4715, for each PC. We also obtained the bolometric photon luminosity over the total polar cap *via* a finite element (particle tracing) approach and integrating numerically over all energies and field lines from the surface to the light cylinder

$$L_\gamma = \int_0^{\Theta_0}\int_0^{2\pi}\left(\dot{N}(\phi,\theta)\int_{r=R}^{r=c/\Omega} P_\gamma(\phi,\theta,r(t))\,dt\right)d\phi\,d\theta. \qquad (7)$$

Here P_γ is the CR photon power integrated over frequency, $\dot{N} = \rho_{\rm e} c dS/e$ the number of particles ejected per second from a PC surface patch dS centered at (ϕ, θ), and $\rho_{\rm e}$ the charge density. Since we cannot start with an initial velocity equal to c (i.e. infinite Lorentz factor), we assumed values close to c and found convergent photon luminosities of 6–7% (of the spindown power) corresponding to injection velocities of $0.9c$ and $0.99999c$, respectively (also depending on the assumed magnetic field strength, stellar radius and moment of inertia). This agrees closely with our analytical expression for the total electron luminosity of 7% – i.e. almost all particle luminosity is converted to photon luminosity as expected for strong radiation reaction. It should however also be noted that the fundamental expression for $E_{||}$ (unscreened) changes sign along ~40% of the field lines originating at the polar cap (see Figure 3).

We expect the system to reach a steady state as a result of the redistribution of charges along field lines corresponding to electric field reversals. These field lines are then expected to become equipotential lines, or, a reduced current for this region may develop, resulting in the suppression of particle acceleration along them. This justifies our neglect of these field lines (for which field reversals occur) when calculating the pulse profile, bolometric photon luminosity, and observer time-averaged integral flux.

For the classical case, the efficiency of converting spindown power into photon luminosity is ~90%, but this factor is highly uncertain due to the large uncertainty in electric potential for the classical case.

The differential photon power $dL_\gamma(E)/dE$ is obtained by inserting the ratio of the indicator function $I(E, E + dE)$ and the selected energy bin width dE in the integrand of Eq. (7). This allows us to compare the expected integral photon flux with EGRET (Fierro et al., 1995) above 100 MeV and 1 GeV, as well as proposed H.E.S.S. observations of this pulsar (Venter, 2004). Note that the imaging threshold

energy of H.E.S.S. is ∼100 GeV (Hofmann, 2001), although a non-imaging "pulsar trigger" for timing studies down to $\gtrsim$30 GeV can be employed for pulsar studies with H.E.S.S. (de Jager et al., 2001).

Since most of the power is radiated into a cone with half emission angle θ_B (the polar tangential angle at the emission point of the maximum CR energy), we can express the instantaneous polar cap averaged flux at a distance $d = 139$ pc to Earth as

$$F_\gamma^{\rm PC}(>E) = \frac{1}{\Delta\Omega d^2}\int_E^\infty \frac{1}{E'}\left(\frac{dL(E')}{dE'}\right)dE'. \tag{8}$$

The beaming solid angle is selected to correspond to energies above $E = 100$ MeV, giving

$$\Delta\Omega(>E) = 2\pi(1-\cos\theta_B) \sim 0.5 \text{ sr} \tag{9}$$

per polar cap, resulting in a phase-averaged photon flux (as would be seen on a DC skymap) for a single polar cap corresponding to

$$\bar{F}_\gamma(>E) = 2\phi_L F_\gamma^{\rm PC}, \tag{10}$$

with $2\phi_L \sim 0.2$ the pulse width corresponding to the bulk of this emission (see Figure 1). The stated values of $\Delta\Omega(>E)$ and $2\phi_L$ correspond within 20% to the range of values found for the range of assumed values of the polar cap magnetic field strengths, radii and moments of inertia. Only one polar cap is expected to be seen, given the relative orientations of the magnetic axis and observer line-of-sight to the spin axis. The radial coordinate at the position of maximum CR energy $\eta_{\rm m}$, as well as $2\phi_L/\Delta\Omega$, are independent of the choice of injection velocities up to $\sim 0.9999c$.

Figure 1 shows the pulse profile for an observer sweeping at an inclination angle of 40° relative to the spin axis, while the magnetic axis is tilted by an angle of $\chi = 35°$ relative to the spin axis (Manchester and Johnston, 1995). Only half a period is shown, with phase zero ($\phi_L = 0$) corresponding to the closest approach with respect to the magnetic axis, at which the observer is at an angle of $40° - \chi \sim 5°$ relative to the magnetic axis.

A value of $2\phi_L/\Delta\Omega = 0.4$ was used throughout (see Figure 2). The energy spectrum dL/dE is quite hard, resulting in a hard time-averaged photon flux $\bar{F}_\gamma(>E)$, as shown in Figure 2 for two values of the polar cap magnetic field strength and two (R, I) combinations indicated on the figure. It is clear that the EGRET upper limit at 100 MeV is most constraining, resulting in an upper limit of $B_8 < 4$ for $R_6 = I_{45} = 1$, but $B_8 < 1$ for $R_6 = 1.6$, $I_{45} = 3$.

Strong radiation reaction near the pulsar surface, combined with further (weak) acceleration towards the light cylinder, result in a total residual electron power of $\sim 0.05\dot{E}_{\rm rot}$ at the light cylinder.

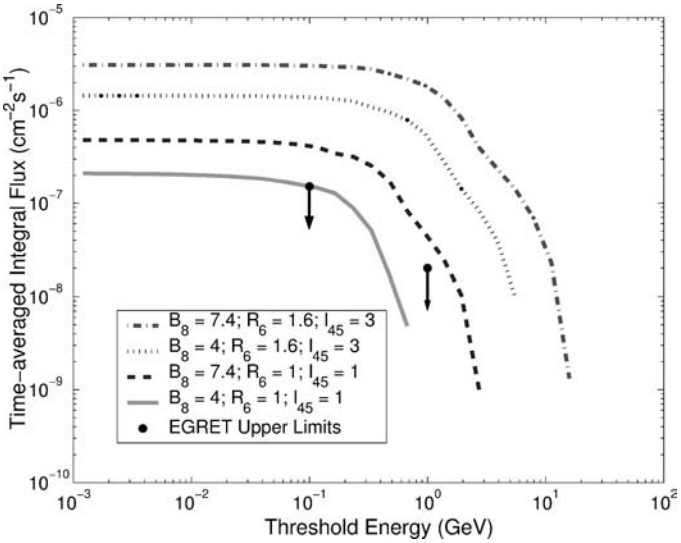

Figure 2. Observer time-averaged integral flux vs. threshold energy for different polar cap magnetic field strengths ($B_8 = B_{\rm pc}/10^8$ G), stellar radii ($R_6 = R/10^6$ cm) and moments of inertia ($I_{45} = I/10^{45}$ g cm^2) as indicated in the legend. These results are invariant (within 10%) for injection speeds corresponding to the range $0.9 < \beta_0 < 0.99999$ and $2\phi_L/\Delta\Omega = 0.4$. The EGRET upper limits are also indicated.

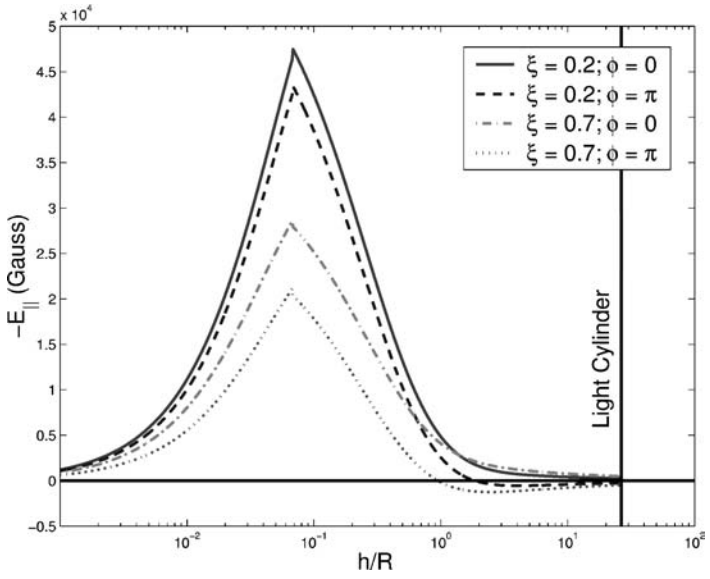

Figure 3. Electric field component parallel to the magnetic field vs. scaled height above the stellar surface for $B_8 = 4$, $R_6 = 1$, and $I_{45} = 1$. Note the sign reversal for $\phi = \pi$.

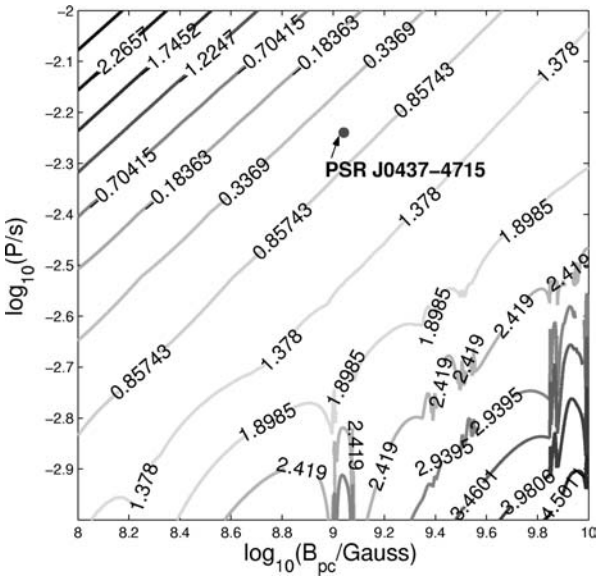

Figure 4. Contour plot of the maximum CR photon energy (labelled as $\log_{10}(E_{\rm CR}^{\rm max}/1\ {\rm GeV})$) vs. $\log_{10}(P/{\rm s})$ and $\log_{10}(B_{\rm pc}/{\rm Gauss})$. No magnetic pair production is expected to take place for the parameter ranges shown in the figure. We used $R_6 = 1$, $\chi = 45^\circ$ and $M = 1.4 M_{\rm sun}$. (It seems as though the model has some numerical instability at smaller periods and larger magnetic fields).

3.2. Spectral cutoffs for millisecond pulsars due to GR frame dragging

The maximum CR energies for millisecond pulsars were calculated from the finite element approach described earlier and plotted as contours in Figure 4. The period range corresponds to 0.001–0.01 s, whereas polar cap field strengths of 10^8–10^{10} G were selected.

The position of PSR J0437-4715 is also indicated on the figure (corresponding to an energy near 4 GeV for the assumed parameters indicated in the figure caption). The highest energies correspond to the smallest periods and largest field strengths, where screening may start to take place according to the model of HMZ02. Most millisecond pulsars are however expected to have unscreened magnetospheres, for which the earlier results apply.

4. Conclusions

CR cutoff energies for millisecond pulsars such as PSR J0437-4715 were predicted to be in the range 50–100 GeV by HMZ02 and Bulik et al. (2000), making proposals for ground-based telescopes with imaging thresholds near 100 GeV (e.g. H.E.S.S. (Hofmann, 2001) and CANGAROO (Yoshida et al., 2002)) attractive. From the present GR theory it appears as though these telescopes may not be able to see the

spectral tail corresponding to the intense primary CR component, since the hard primary CR spectrum does not extend to energies above $\sim$20 GeV, as verified by both analytical and numerical (finite element) approaches. An inverse Compton component resulting from TeV electrons scattering the UV/soft X-ray photons from the surface of PSR J0437-4715 may however still be detectable, although this prediction by Bulik et al. (2000) should be re-evaluated within a GR electrodynamical framework.

Even the EGRET upper limit above 100 MeV appears to be constraining: the polar cap field strength should be less than 4×10^8 G, with the exact limit depending on the equation of state. Furthermore, Fierro et al. (1995) analysed EGRET data up to 1995, whereas the full EGRET data set of this pulsar (including observations beyond 1995) should be reanalysed, using the additional *a priori* information of testing for a 20% duty cycle in phase with the radio pulse, which should lead to even more constraining flux upper limits than those presented here.

Future refinements should include incorporation of the GR-corrected magnetic field (or even multipoles instead of a dipole – see Navarro et al. (1997)), the GR curvature radius, making more appropriate assumptions concerning the primary electrons' initial velocities (Sakai and Shibata, 2003) and treating the field reversals properly. Also, cuts through the PC made by the observer should be modelled in detail, instead of using averaged values for the solid angle and duty cycle.

References

Bulik, T., Rudak, B. and Dyks, J.: 2000, *MNRAS* **317**, 97.

de Jager, O.C., Konopelko, A., Raubenheimer, B.C. and Visser, B.: 2001, *Am. Inst. Phys.* **558**, 613.

Dyks, J., Rudak, B. and Bulik, T.: 2001, Proceedings of the 4th Integral Workshop, A. Gimenez, V. Reglero and C. Winkler (ESA SP-459, Noordwyk) (eds.), p. 191.

Fierro, J.M., et al.: 1995, *ApJ* **447**, 807.

Harding, A.K. and Muslimov, A.G.: 1998, *ApJ* **508**, 328

Harding, A.K., Muslimov, A.G. and Zhang, B.: 2002, *ApJ* **576**, 366 (HMZ02).

Hofmann, W.: 2001, Proceedings of the 27th ICRC, Hamburg, vol. OG2.5, p. 2785.

Johnston, S., et al.: 1993, *Nature* **361**, 613.

Luo, Q., Shibata, S. and Melrose, D.B.: 2000, *MNRAS* **318**, 943.

Manchester, R.N. and Johnston, S.: 1995, *ApJ* **441**, L65.

Muslimov, A.G. and Harding, A.K.: 1997, *ApJ* **485**, 735.

Muslimov, A.G. and Harding, A.K.: 2003, *ApJ* **588**, 430.

Muslimov, A.G. and Tsygan, A.I.: 1992, *MNRAS* **255**, 61.

Navarro, J., Manchester, R.N., Sandhu, J.S., Kulkarni, S.R. and Bailes, M.: 1997, *ApJ* **486**, 1019.

Sakai, N. and Shibata, S.: 2003, *ApJ* **584**, 427.

Usov, V.V.: 1983, *Nature* **305**, 409.

Van Straten, W., Bailes, M., Britton, M.C., Kulkarni, S.R., Anderson, S.B., Manchester, R.N. and Sarkissian, J.: 2001, *Nature* **412**, 158.

Venter, C.: 2004, *M.Sc. thesis*, North-West University, Potchefstroom, unpublished.

Yoshida, T., Yoshikoshi, T. and Yuki, A.: 2002, *Astropart. Phys.* **16**, 235.

Zavlin, V.E., Pavlov, G.G., Sanwal, D., Manchester, R.N., Trümper, J., Halpern, J.P. and Becker, W.: 2002, *ApJ* **569**, 894.